Journal of Mining and Environment (JME) Vol. 17, No. 1, 2026, 295-308

Shahrood University of Technology

Journal of Mining and Environment (JME)

Journal homepage: www.jme.shahroodut.ac.ir

Iranian Society of Mining Engineering (IRSME)

The Effects of Mineral Size, Texture Coefficient (TC), and Ductility-Brittleness on Creating Hole in Granitic Rock Specimens

Aram Ardalanzdeh[1], Seyed Davoud Mohammadi[1]*, Vahab Sarfarazi[2], and Hossein Shahbazi[1]

1. Department of Geology., Bu-Ali Sina University, Hamedan, Iran
2. Department of Mining Engineering., Hamedan University of Technology, Hamedan, Iran

Article Info

Received 19 October 2024

Received in Revised form 8 December 2024

Accepted 19 December 2024

Published online 19 December 2024

DOI: 10.22044/jme.2024.15230.2913

Keywords

Keywords: Granite

Rock texture

Rock Hole

Texture Coefficient

Brittleness Index

Abstract

Creating holes in rocks using different methods presents various challenges. In this research, an attempt was made to investigate these characteristics and the existing problems in creating holes based on the texture and brittleness of the rock. For this purpose, several core specimens were taken from the Alvand granitic batholith of Hamadan, and the petrological and textural indexes of the rocks were determined. There are four types of rock textures, ranging from coarse-grained to fine-grained. The texture coefficients (TC) for the four types of rocks (G1 to G4) were 1.709, 1.730, 1.774, and 1.697, respectively. The brittleness index (B1) for the four types of rocks (G1 to G4) were 9.13, 11.01, 12.07, and 10.65, respectively. After that, using a diamond drill, one hole was created in each rock core specimen, and at the end of drilling, a fracture pit was separated from the bottom of each hole in the specimen. The results show that as the mineral size decreases, the fracture pit depth also decreases, and in porphyry texture, the fracture pit depth is between the fracture pit depths of coarse-grained and medium-grained rocks. As the texture coefficient (TC) and brittleness of the rock specimens increase, the fracture pit depth decreases, and in porphyry texture, the fracture pit depth remains between the fracture pit depths of coarse-grained and medium-grained rocks. Finally, the results from laboratory tests indicate that creating holes using a drill to study the effect of the holes on rock behavior can cause damage to the rocks.

1.Introduction

Rock is a natural material, composed of various minerals and formed through long-term geological processes. The differences in properties among its components and internal micro fissures determine the mesoscopic heterogeneity of rock, which is the basis cause for the differences in the failure of different rock types. Ductility usually means the material can maintain a complete and continuous deformation property. In contrast, brittleness means that the material loses continuity and the initiation and expansion of cracks occur [1]. The brittleness characteristics of rock have important guiding significance for hard rock resource exploitation, rock burst prediction, mechanical excavation efficiency, and unconventional oil and gas resource exploitation [2-5]. The mechanical properties of rocks with different types of defects vary greatly compared with intact rocks [6-11]. Determination of the mechanical behavior of intact rock is one of the most important parts of any engineering project in the field of rock mechanics [12]. To understand the stability of deep underground engineering rocks at high temperatures, it is necessary to conduct comprehensive tests on the mechanical properties of the rocks. Various fractures and holes in the natural rock mass affected the mechanical properties of the rock mass and the safety construction of engineering [13]. Safari et al. [14] investigated the effect of the petrography, mineralogy, and physical properties of limestone in dry and saturated conditions. The brittle-ductile transition and nonlinear deformation behaviors are

Corresponding author: d.mohammadi@basu.ac.ir (S.D. Mohammadi)

the prominent characteristics of the rock. Rocks transition in failure mode ranges from localized brittle fracture to non-localized plastic flow. This transition plays a significant role in various geophysical and geological problems. The mechanical behavior of rocks in the brittle-ductile transition region is restricted by strain rate, temperature, effective stress, the microstructure, porosity, and mineralogy of the rock and water [15-22]. The brittle behavior of rock is a necessary condition for engineering disasters such as spalling and rock bursts in the deep surrounding rock, and the higher the brittleness is, the greater the tendency of the above disasters to occur [23-29]. Under external loading, the change in the mechanical properties of defective rock samples is a complex process, depending on the properties of the rock block and the internal defects of the rock mass [30-31]. Rock brittleness is a key parameter determining the failure characteristics of rocks upon loading and unloading conditions. Several mechanical responses and failure processes of rocks, such as cutability and drillability, are associated with rock excavation [32-33]. The study on the brittle–ductile mechanical properties of rocks can help to deep mine's rock-burst prediction and prevention and has significant engineering significance [34]. The effects of fracturing on the strength and stress–strain curves of the pre-cracked rock-like materials have been discussed. It has been shown that the crack propagation mechanism in brittle substances due to the crack's coalescence phenomenon occur mainly by propagation of wing cracks emanating from the tips of the pre-existing cracks. The secondary cracks may also be produced after the propagation of the wing cracks in the specimens under uniaxial loadings but it is experimentally shown that the wing cracks are mainly responsible for the cracks coalescence and the final cracks propagating paths [35]. The mechanism of crack propagation in concrete specimens containing cracks under shear loading conditions has been studied. The coalescence mechanism of cracks indicated that the pre-cracked concrete failure occurs in mixed mode in case of non-overlapping cracks configuration and in tensile mode for the overlapping cracks. Finally, comparing the numerical and experimental results validated the crack propagation modeling and verified the accuracy and efficiency of the proposed numerical method [36]. The mechanism of cracks propagation and coalescence of neighboring cracks existing in pre-cracked rock like cylindrical specimens has been studied experimentally and numerically by considering multiple cracks in the middle part of each specimen. The crack propagation and coalescence paths of the internal inclined crack are estimated by implementing a suitable iteration algorithm of incremental crack length extension in a direction predicted by using the maximum tangential stress criterion [37]. Haeri and Sarfarazi [38] have studied the deformable multilaminate for predicting the Elasto-Plastic behavior of rocks. In the mentioned paper, a multilaminate-based model has been developed and presented to predict the strain hardening behavior of rock. In this multilaminate model, the stress–strain behavior of a material is obtained by integrating the mechanical response of an infinite number of predefined oriented planes passing through a material point.

In addition, many scholars have studied and analyzed the mechanical properties of rock, such as crack propagation and failure criterion, using physical tests, and many meaningful results have been obtained [39-44]. Brittleness is a very considerable mechanical property of intact rocks because it causes strong impacts on the rock fracturing process and failure behaviors [45]. The brittle-ductile transition and nonlinear deformation behaviors are the prominent characteristics of the rock. Rocks transition in failure mode ranges from localized brittle fracture to non-localized plastic flow. This transition plays a significant role in various geophysical and geological problems. The mechanical behavior of rocks in the brittle-ductile transition region is restricted by strain rate, temperature, effective stress, the microstructure, porosity, and mineralogy of the rock and water [46-58]. Contact problem and pre-cracks in some materials have been investigated by many researchers. Yaylaci et al. [59-61] have investigated the punching phenomena in soft and rigid materials and their contact problems. In this research, the effects of texture coefficient (TC), ductility-brittleness and mineral size on creating hole by diamond drill in granitic rock specimens were investigated.

2. Geology setting

Alvand batholith is located in the south and west of the Hamedan region and the northern part of the Sanandaj-Sirjan transformation zone. Its length is about 40 km and its width reaches 10 km. Alvand batholith is almost oval in shape, but its central part is narrow and its two sides are bulky. The age of this mass goes back to 64 to 70

million years ago and in the earlier Paleocene [62]. The Alvand pluton is a composite consisting of gabbroic rocks, granites, including mylonitized varieties, and leuco-cratic granitoids that occupy an area of ~ 800 km^2 [63]. From the point of view of geology, the Hamedan region is a part of the Sanandaj-Sirjan structural zone, which is located at the border of Central Iran and Zagros zones with the general trend of the North-West-South-East. The origin of granite and gabbro parts of the mass has been studied by different researchers. Valizadeh and Cantagrel [64] considered the granite rocks of Alvand to be S-type according to mineralogical, geochemical and geological characteristics and introduced the gabbroic part as older than the granite part and due to the presence of secondary biotites in the gabbroic rocks, the impact Alvand granite has been proposed on the basic rocks of Cheshme Qasaban and North Sarkan. Eshraghi and Mohammadi Gharai [65] relates the intermediate rocks of Alvand to the process of metasomatism related to the effect of granitic fluids on gabbros. Alvand plutonic complex consists of various lithological units from mafic, intermediate to felsic rocks. According to some researchers, this zone is a part of the orogenic belt of Zagros. The lower unit of the Hamedan metamorphic complex comprises variably deformed and metamorphosed pelitic, semipelitic and psammitic metasediments as well as quartzite, amphibolite and hornblende garben schists and some calc-silicate rocks [66-67].

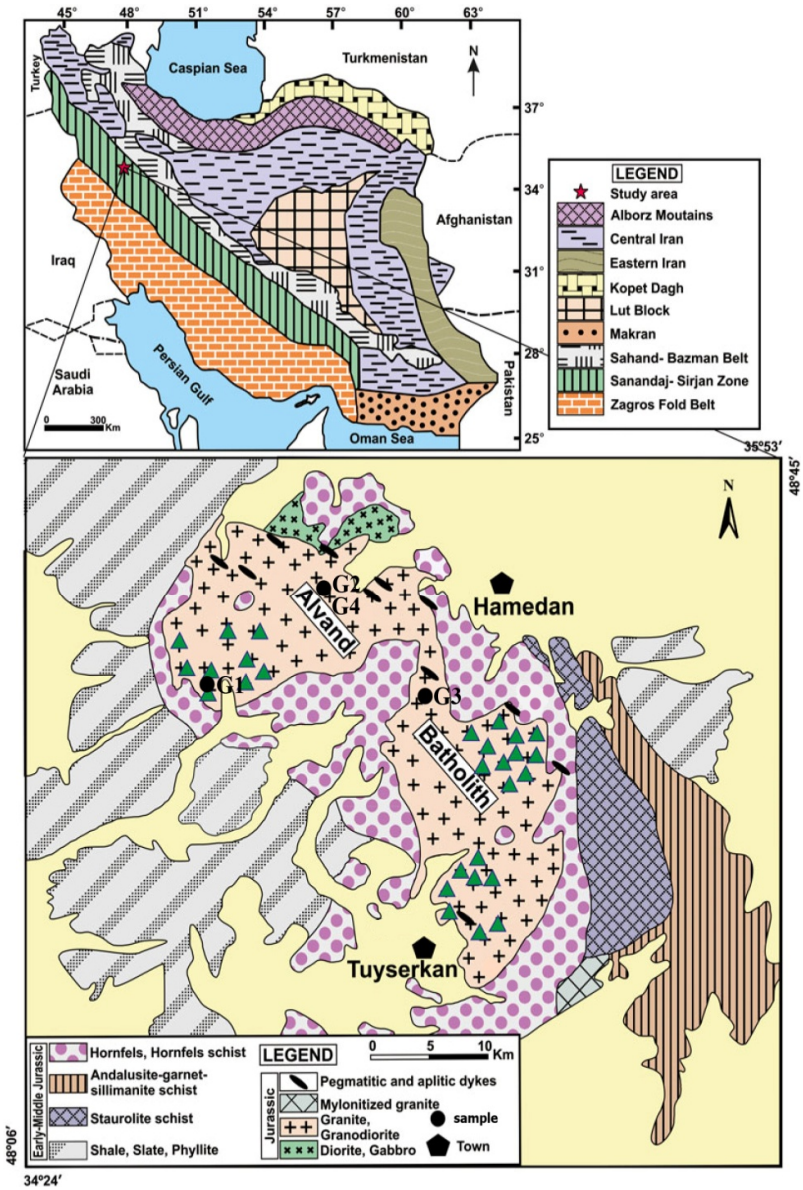

Figure 1. Lithotectonic map of Iran [68] and simplified geo-logical map of the Hamedan region [69].

3. Materials and Methods

3.1. Sampling and preparing of core specimens

The rock blocks used in this research with dimensions of about 40×30×30 cm were collected from the exposed granitic rocks of the Alvand batholite from the Kahnoosh village, Ganjnameh and Imamzadeh Hassan regions (Table1). The Rock block samples were transferred to the laboratory of Bu-Ali Sina University to be prepared and laboratory tests performed on them. To prepare the specimens, cores with diameters of 64 and 66 mm and length to diameter ratio (L/D) greater than 2 were prepared from each type of rock. The beginning and end of the specimens were completely smooth and uniform (Figure 2).

To prepare the specimens, after taking the core, an initial hole was created in the specimens using a 5 mm diameter drill, then the hole diameter was increased using a 10 mm diameter drill. Finally, the diameter of the hole increased to 15 mm (Figure 3). The rotation rate of the drill and the penetration rate are equal to 120 RPM and 5 mm/min, respectively. It is worth noting that the time taken for each sample preparation (G1 to G4) was 4, 7, 11, and 9 minutes, respectively.

Figure2. Rock coring and preparing in the laboratory

Figure 3. Final specimens prepared from four types of rock with different hole diameters

3.2. Physical and mechanical properties of rock specimens

To determine the physical and mechanical properties of the specimens, UCS, specific gravity, moisture percentage, and porosity tests were performed and the results obtained were averaged for three specimens, which are as described in Table 2. The highest specific weight was related to specimen G4 and the lowest was related to specimen G1. The moisture percentage of the specimens was less than one percent and the porosity of the specimens was close to zero.

Table1. Sampling dimensions and location

Rock specimen	Dimensions of the sample (mm)		Rock textures	Sampling location	Coordinates (UTM)	
	Diameter	length			X	Y
G1	66	144	Coarse-grained	Kahnoosh village	249678	3844730
	66	148				
	66	148				
G2	64	129	Medium-grained	Ganjnameh	265705	3848129
	64	136				
	66	146				
G3	64	130	Fine-grained	Imamzadeh Hassan	260971	3852148
	64	134				
	64	140				
G4	64	128	porphyry	Imamzadeh Hassan	261079	3852625
	64	132				
	64	136				

Table 2. Physical and mechanical properties of rock specimens

Rock specimen	UCS (MPa)	σ_t (MPa)	$(\frac{\sigma_c}{\sigma_t})$	E (GPa)	γ (gr/cm^3)	γ_d (gr/cm^3)	γ_{sat} (gr/cm^3)	ω (%)	e	Gs
G1	39	4.27	9.13	27	2.50	2.50	2.52	0.23	0.01	2.50
G2	99	8.99	11.01	92	2.62	2.62	2.64	0.02	0.00	2.62
G3	118.5	9.82	12.07	77	2.60	2.60	2.61	0.16	0.00	2.60
G4	111	10.42	10.65	69	2.74	2.73	2.74	0.12	0.00	2.73

G1= Coarse-grained, G2= Medium-grained, G3= Fine-grained, G4= porphyry, UCS: Uniaxial compression strength, σ_t: Brazilian tensile strength, E: Young's modulus, γ:density, γ_d :Dry density, γ_{sat}: saturation density, ω: Moisture percentage, e:porosity ratio, Gs: specific gravity.

3.3. Mineralogy characteristics of rock specimens

From each specimen, a thin section was prepared to study the mineralogical characteristics, and images were prepared and studied using a microscope with 4x magnification and XPL. Specimen G1 consists of orthoclase, quartz, biotite, plagioclase, muscovite, and zircon in order of abundance. Specimen G2 is composed of plagioclase, quartz, sphene, muscovite and zircon minerals in order of abundance. Specimen G3 is composed of quartz, alkali feldspar, biotite, muscovite and plagioclase minerals in order of abundance. Specimen G4 is composed of quartz, plagioclase, biotite, muscovite and amphibole in order of abundance (table 3).

Table 3. The percentage of minerals in the studied rocks

Rock specimen	Orthoclase (%)	Quartz (%)	Biotite (%)	Plagioclase (%)	Muscovite (%)	Zircon (%)	Alkali feldspar (%)	Sphene (%)
G1	40	25	15	10	5	5	---	---
G2	---	40	---	39	5	1	---	15
G3	---	40	15	5	5	---	35	---
G4	---	45	20	20	15	---	---	---

G1= Coarse-grained, G2= Medium-grained, G3= Fine-grained, G4= porphyry

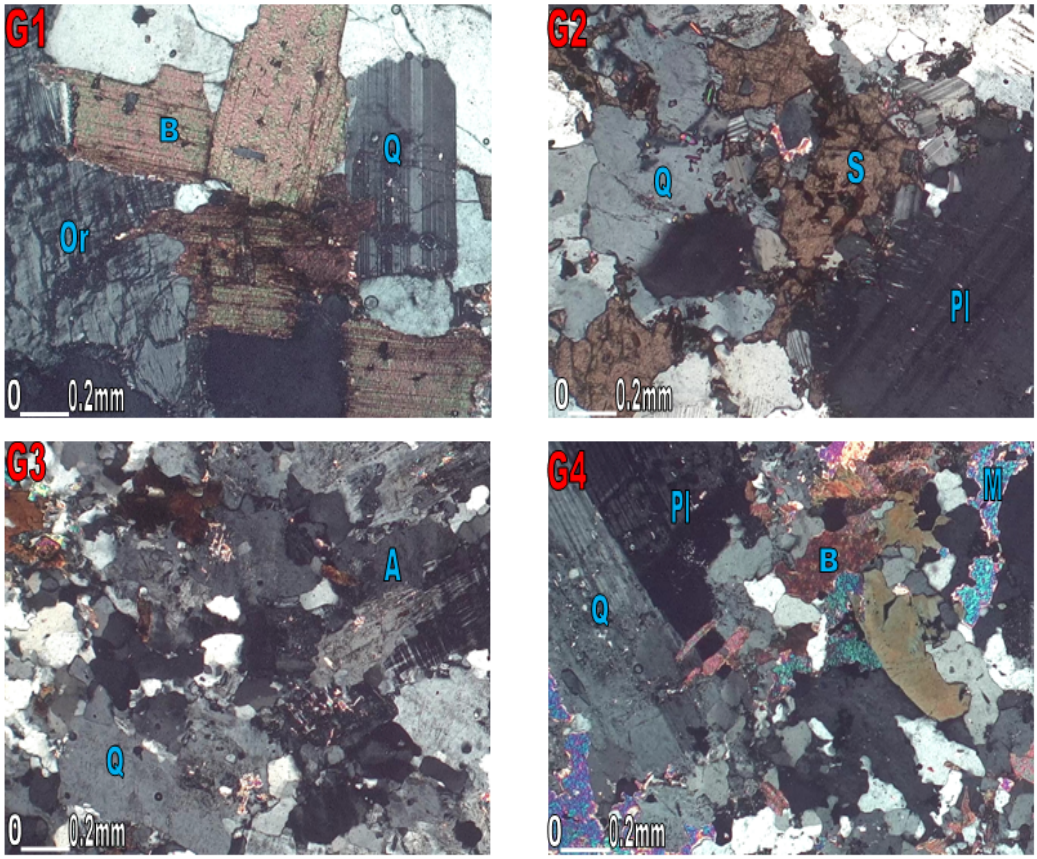

Figure 4. Microphotographs of G1= Coarse-grained, G2= Medium-grained, G3= Fine-grained, G4= porphyry, Or=Orthoclase, Q= Quartz, B= Biotite, Pl= Plagioclase, M= Muscovite, Z= Zircon, A=alkali feldspar, S= Sphene.

3.4. Petrological and Textural Indexes

3.4.1. Texture Coefficient

Microtextural features influence the petrophysical and mechanical properties of rocks, including the elastic properties and cracking processes under axial loads [70]. The rock texture or micro-fabric studies have an important role to find which factors are significant or underestimate in rock mechanics. Also, many practical rock mechanics studies rely on basic geological or microscopic studies [71]. It is now possible to digitalize the image of a rock thin section and use it to analyze its texture in order to measure a characteristic value that represents it [72-73]. One way to quantify rock texture is using a texture coefficient (TC) method. One of the first methods for quantification of rock texture was proposed by Howarth and Rowlands [74]. Many researchers have proposed TC as a good way to predict some geotechnical properties and classify different rocks [75-78].

Rock texture can be quantified using the geometrical features and interlocking index or packing density of the grains about the matrix effect. Grain shape and size can be quantified by the length (L), width (W), area (A), and perimeter (P), which are used to formulate several coefficients such as the aspect ratio (AR; Eguation 1) and form factor (FF; Eguation 2). For circle and equilateral polygon shapes, the AR was equal to 1, but for other grain shapes, AR was greater than 1. The FF decreased when the roughness and elongation of grains were increased. Packing density can also be quantified using area weighting of grains (AW; Eguation 3), which is the relative proportion of matrix and grains. The angle factor (AF) is used to quantify the angular orientation of grains and is calculated only for elongated grains (AR > 2). The AF is computed using a class-weighted system applied to the acute angular differences between elongated grains (Eguation 4). The angular differences are categorized into nine classes, each of which is weighted (e.g., class 1 is 0–10 ° and is weighted by 1, class 2 is 11–20 ° and weighted by 2, etc., with the last class being 81–90 ° and weighted by 9).

$$AR = \frac{L}{W} \tag{1}$$

$$FF = \frac{4\pi A}{P^2} \tag{2}$$

$$AW = \frac{\sum(\text{Grain area within the reference area boundary})}{(\text{Area boundary by the reference area})} \tag{3}$$

$$AF = \sum_{i=1}^{9}\left(\frac{x_i}{\frac{N(N-1)}{2}}\right) \times i \tag{4}$$

where N is the total number of elongated particles and xi is the number of angular differences in each class [80]. High values of these factors can be interpreted as a rock texture that influences the geotechnical properties. The quantitative assessment of rock texture is formulated using these factors in Eguation 5[72].

$$T_c = AW\left[\left(\frac{N_0}{N_0+N_1} \times \frac{1}{FF_0}\right) + \left(\frac{N_0}{N_0+N_1} \times AR_1 \times AF_1\right)\right] \tag{5}$$

where N_0 and N_1 are the numbers of grains whose AR is below and above a pre-set discrimination level (defined as 2), respectively; FF0 and AR1 are the arithmetic mean of discriminated FF and AR, respectively; and AF1 is proposed to divide the AF value by 5 (AF1 = AF/5). The application procedure details of the TC method are described by Howarth and Rowlands [74].

It has been noted that engineering properties of rocks (such as uniaxial compressive strength, Brazilian tensile strength, Young's modulus, density, shore hardness, porosity, and point load index) are enhanced when the TC value is increased [75-78]. Therefore, TC can be used to find correlations between engineering properties and rock texture.

It is possible to calculate the TC according to the thin sections of rock in two main ways: (i) calculating manually; and (ii) using image analysis of the rock thin section [74]. In current study, last method for calculating TC was used (Figure5).

In this method, pictures (in TIF format) of rock thin sections are prepared and analyzed using JMicroVision v.1.27 software, which has been developed specially to analyze high-definition images of rock thin sections and contains tools for either manual or automatic quantification [79].

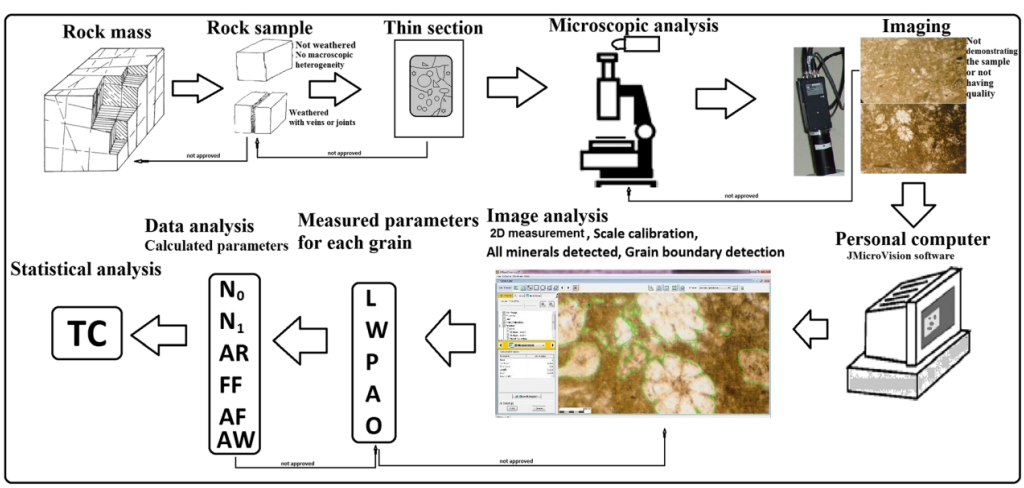

Figure5. Method of determining the texture coefficient (TC). A is an area, AF is angle factor, AR is aspect ratio, AW is area weighting of grains, FF is form factor, L is length, N0 and N1 are the numbers of grains whose aspect ratio is below and above a pre-set discrimination level (defined as 2), respectively, O is orientation, P is perimeter, W is width [78].

3.5. Ductility-brittleness Indexes

Brittleness is an important parameter controlling the mechanical behavior and failure characteristics of

rocks under loading and unloading conditions, such as fracability, cutability, drillability and rockburst

proneness [5]. The term "brittle" or "brittleness" is often qualitatively used to describe the response and behavior of rocks under different loading conditions (tension, compression, or indentation) Figure 6.

The Brittleness index is often determined based on Brazilian tensile strength (BTS) and uniaxial compressive strength (UCS) of rock in engineering practice [79-84]. In this study, three common brittleness definitions include Eguation 6 and 7 [83] and Eguation 8 [85] Table 5,

$$B_1 = \frac{\sigma_c}{\sigma_t} \tag{6}$$

$$B_2 = \frac{\sigma_c - \sigma_t}{\sigma_c + \sigma_t} \tag{7}$$

$$B_3 = \frac{\sigma_c \times \sigma_t}{2} \tag{8}$$

where σ_c and σ_t are the uniaxial compressive strength (UCS) and Brazilian tensile strength, respectively. It is generally believed that the higher the values of B, the more brittle the rock. The values B_1 and B_2 are popularly used for the assessment of rock fragmentation efficiency [86-87].

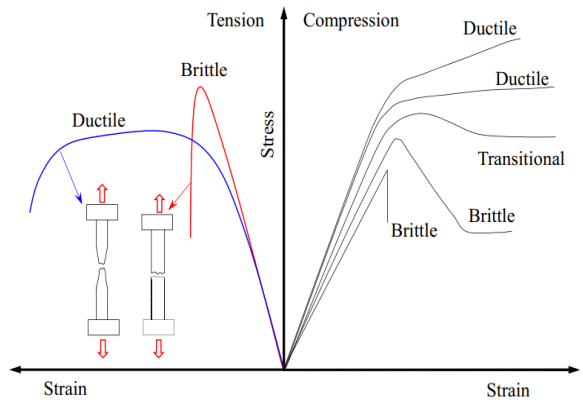

Figure6. Brittle and ductile behavior of material under tension (the left half) and compression (the right half) loading conditions. The right part shows the brittle and ductile behavior of trachyte under different confining pressures [83].

4. Results and Discussions

As mentioned earlier, holes with diameters of 5 mm, 10 mm, and 15 mm were created in the cores using a diamond drill. As shown in Figure 7, at the end of the drilling process, a fracture pit was formed, and a piece of rock separated from the back of the specimens.

Figure7. Fracture pits were formed in the granitic rock core specimens

The following are the results of the relationship between fracture pit depth, texture coefficient (TC), and ductility-brittleness for granitic rock specimens.

4.1. Relationship between fracture pit depth and mineral size

There are four types of textures: coarse-grain, medium-grained, fine-grained, and porphyry. The depths of the fracture pits are 3.5 cm for coarse-grained granitic rocks, 2.5 cm for medium-grained granitic rocks, 1.5 cm for fine-grained granitic rocks, and, 3 cm for porphyritic granitic rocks. The results showed that as the dimensions of the mineral increase, the depth of the fracture pit also increases, but in porphyry texture, the fracture pit depth remains between the fracture pit depths of coarse-grained and medium-grained rocks.

4.2. Relationship between fracture pit depth and TC

The results of texture coefficient (TC) and its parameters are shown in Table 4.

Table 4. Results of texture coefficient (TC)

Rock specimen	N0	N1	FF0	AR	AF	AW	TC
G1	73	27	0.675	2.469	0.943	1	1.709
G2	33	181	0.666	2.297	0.771	1	1.730
G3	144	21	0.594	2.417	0.992	1	1.774
G4	228	43	0.642	2.392	1.018	1	1.697

G1= Coarse-grained, G2= Medium-grained, G3= Fine-grained, G4= porphyry

The investigation of TC shows that in coarse-grained to fine-grained (G1 to G3) specimens, the TC increased, while in porphyry texture (G4), the TC decreased. Additionally, with increasing TC, the depth of the fracture pit after creating the hole in granitic rock cores decreased, except for the porphyry texture (G4).

4.3. Relationship between fracture pit depth and ductility-brittleness

The results of brittleness are shown in table 5.

Table 5. Computed brittleness values of the rock specimen

Rock specimen	B_1	B_2	$B_3(MPa)^2$
G1	9.13	0.80	83.26
G2	11.01	0.83	445.00
G3	12.07	0.85	581.83
G4	10.65	0.83	578.31

G1= Coarse-grained, G2= Medium-grained, G3= Fine-grained, G4= porphyry

The investigation of brittleness values shows that in coarse-grained to fine-grained (G1 to G3) specimens, the B_1, B_2, and B_3 values increased, while in porphyry texture (G4), the brittleness indexes decreased. Additionally, with increasing brittleness indexes, the depth of the fracture pit after creating the hole in granitic rock cores decreased, except for the porphyry texture (G4).

5. Conclusions

The investigation was carried out on four types of textures: coarse-grained, medium-grained, fine-grained, and, porphyry. With increasing the minerals size of granitic rocks, the rock strength was decreased. With increasing the TC, rock strength, and ductility were increased. With increasing the minerals size, the ductility of the rock was increased. With the increase of the brittleness indexes, the strength of the rock increased and the ductility of the rock decreased. The results showed that at the end of drilling, a fracture pit is separated from the back of the specimen. In granitic rocks with porphyry texture, the fracture pit depth remains between the fracture pit depths of coarse-grained and Medium-grained rocks (table 6).

As seen in Table 6, B1 and Tc are important parameters for creating fracture pits. In laboratory tests that require drilling holes to study the effect of the holes on rock properties, the use of a drilling machine causes damage to the rocks. In large scale, this phenomenon can occur in rock masses, and drilling machines such as T.B.M. can cause fracture pits around the created tunnels. Of course, this issue requires further study in large-scale projects. Finally, regarding the fracture pits created during the drilling of rock cores with various textures, it is recommended to use alternative methods, such as the water jet method, to create holes in order to avoid fracture pits and disturbances in the rocks.

Table 6. Relationship between TC, B_1 and fracture pit in granitic rocks

TC / B_1	Coarse-grained (G_1), TC=1.709, Depth of fracture pit=3.5 cm	Medium-grained (G_2), TC=1.730, Depth of fracture pit=2.5 cm	Fine-grained (G_3), TC=1.774, Depth of fracture pit=1.5 cm	Porphyry (G4), TC=1.697, Depth of fracture pit=3 cm
9.13	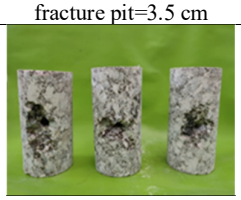			
11.01				
12.07				
10.65				

Conflict of Interest

The authors declare that they have no conflict of interest.

References

[1]. Gonzalez, J., Saldana, M., Arzua, J. (2019). Analytical Model for Predicting the UCS from P-Wave Velocity, Density, and Porosity on Saturated Limestone. *Applied Sciences, 9(23*), 5265.

[2]. Yagiz, S. (2008). Utilizing rock mass properties for predicting TBM performance in hard rock conditions. *Tunneling and Underground Space Technology, 23*, 326–339.

[3]. Yagiz, S. (2009). Assessment of brittleness using rock strength and density with punch penetration test. *Tunneling and Underground Space Technology, 24(1)*, 66-74.

[4]. Kim, T., Hwang, S., Jang, S. (2017). Petrophysical approach for S-wave velocity prediction based on brittleness index and total organic carbon of shale gas reservoir: A case study from Horn River Basin, *Canada Journal of Applied Geophysics, 136*, 513–520.

[5]. Meng, F., Wong, L., Zhou, H. (2021). Rock brittleness indices and their applications to different fields of rock engineering: A review. *Journal of Rock Mechanics and Geotechnical Engineering, 13*, 221–247.

[6]. Zhang, X. P., & Wong, L. (2011). Cracking processes in rock-like material containing a single flaw under uniaxial compression: A numerical study based on parallel bonded-particle model approach. *Rock Mechanics and Rock Engineering, 45(5)*, 711–737.

[7]. Wu, Z., Fan, L., Liu, Q., & Ma, G. (2016). Micro-mechanical modeling of the macro-mechanical response and fracture behavior of rock using the numerical manifold method. *Engineering Geology, 225*. 49- 60.

[8]. Yang, Y., Tang, X., Zheng, H., Liu, Q., & He, L. (2016). Three-dimensional fracture propagation with numerical manifold method. *Engineering Analysis with Boundary Elements, 72*, 65–77.

[9]. Zhang, S., Li, Y., Shen, B., Sun, X., & Gao, L. (2019). Effective evaluation of pressure relief drilling for reducing rock bursts and its application in underground coal mines. *International Journal of Rock Mechanics and Mining Sciences, 114(11)*, 7–16.

[10]. Zhou, S., Zhuang, X., & Rabczuk, T. (2019). Phase field modeling of brittle compressive-shear fractures in rock-like materials: A new driving force and a hybrid formulation. *Computer Methods in Applied Mechanics and Engineering, 355(1)*, 729–752.

[11]. Chen, S., Zhang, J., Yin, D., Cheng, X., & Ning, J. (2021). Relative permeability measurement of coal microchannels using advanced microchip technology. *Fuel, 312*, 122633.

[12]. Davarpanah, M., Somodi, G., Kova´cs, L., Va´sa´rhelyi, B. (2020). Experimental Determination of the Mechanical Properties and Deformation Constants of Mo´ra´gy Granitic Roc Formation (Hungary). *Geotechnical and Geological Engineering, 38(3)*, 3215–3229.

[13]. Wang, Sh., Wang, Li., Ren, B., Ding, K. (2024). Mechanical behavior and fracture characteristics of high-temperature sandstone under true triaxial loading conditions. *Journal of Materials Research and Technology, 28*, 569–581.

[14]. Jiang, N., Lv, K., Gao, Z., Jia, C., Ye, L., Meng, S., Su, Q. (2023). Experimental study on mechanical properties of single fracture-hole red sandstone. *Frontiers in Earth Science, 10*:1083689.

[15]. Safari Farrokhad, S., Lashkaripour, G.R., Hafezi Moghaddas, N., Aligholi, S. (2022). The Effect of the Petrography, Mineralogy, and Physical Properties of Limestone on Mode I Fracture Toughness under Dry and Saturated Conditions. *Applied Sciences, 12(18)*, 9237.

[16]. Liu, W., Zhu, X., & Jing, J. (2018). The analysis of ductile-brittle failure mode transition in rock cutting. *Journal of Petroleum Science and Engineering, 163*, 311–319.

[17]. Aharonov, E., & Scholz, C. (2019). The brittle-ductile transition predicted by a physics-based friction law. *Journal of Geophysical Research: Solid Earth, 124(3)*, 2721–2737.

[18]. Zhao, J., Feng, X., Zhang, X., & Yang, C. (2019). Brittle and ductile creep behavior of Jinping marble under true triaxial stress. *Engineering geology, 258*, 105157.

[19]. Liu, S., Chen, H., Yuan, S., & Zhu, Q. (2020). Experimental investigation and micromechanical modeling of the brittle-ductile transition behaviors in low-porosity. *International Journal of Rock Mechanics and Mining Sciences, 179*, 105654.

[20]. You, T., Waisman, H., & Zhu, Q. (2021). Brittle-ductile failure transition in geomaterials modeled by a modified phase-field method with a varying damage-driving energy coefficient. *International Journal of Plasticity, 136*, 102836.

[21]. Jacquey, A., & Cacace, M. (2020). Multiphysics modeling of a brittle-ductile lithosphere: 2. Semi-brittle, semi-ductile deformation and damage rheology. *Journal of Geophysical Research: Solid Earth, 125(1)*.

[22]. Su, C., Qiu, J., Wu, Q., & Weng, L. (2020). Effects of high temperature on the microstructure and mechanical behavior of hard coal. *International Journal of Mining Science and Technology, 30(5)*, 643–650.

[23]. Kim, B., & Larson, M. (2021). Laboratory investigation of the anisotropic confinement-dependent brittle-ductile transition of a Utahcoal. *International Journal of Mining Science and Technology, 31(1)*, 51–57.

[24]. Cai, M. (2013). Principles of rock support in burst-prone ground. *Tunnelling and Underground Space Technology, 36(6)*, 46–56.

[25]. Eberhardt, E., Lavoie, T., Rahjoo, M. (2020) The importance of geometric dilation in response to brittle rock failure for support design in high stress environments. *In: Rock mechanics for natural resources and infrastructure development—proceedings of the 14th international congress on rock mechanics and rock engineering*, 2509–2516.

[26]. Li, H., Qi, Q., Du, W., Li, X. (2022). A criterion of rockburst in coal mines considering the influence of working face mining velocity. *Geomechanics and Geophysics for Geo-Energy and Geo-Resources, 8(1)*.

[27]. Pan, Y., Wang, J., Zhang, J., Song, Y., Xiao, Y., & Wang, H. (2022). Development and application of a hydraulic impact test machine for simulating rockburst conditions. *Geomechanics and Geophysics for Geo-Energy and Geo-Resources, 8, 105*.

[28]. Zhao, Y., Wang, X., Guo, Y., Danesh, N., & Jiang, Y. (2022a). Mechanical properties and brittleness characteristics of sandstone from different burial depths. *Geomechanics and Geophysics for Geo-Energy and Geo-Resources, 8, 165*.

[29]. Zhao, J., Jiang, Q., Lu, J., Chen, B., Pei, S., & Wang, Z. (2022b). Rock fracturing observation based on microseismic monitoring and borehole imaging: in situ investigation in a large underground cavern under high geo-stress. *Tunnelling and Underground Space Technology, 126(1)*.

[30]. Zhao, J., Jiang, Q., Pei, S., Chen, B., Xu, D, & Song, L. (2023). Microseismicity and focal mechanism of blasting-induced block falling of intersecting chamber of large underground cavern under high geostress. *Journal of Central South University, 30*, 542-554.

[31]. Ulloa, J., Rodrı ´guez, P., Samaniego, C., & Samaniego, E. (2019). Phasefield modeling of fracture for quasi-brittle materials. *Underground Space, 4(1)*, 10–21.

[32]. Xia, Z., Jiang, N., Yang, H., Han, L., Pan, H., Zhao, Z., & Feng, Q. (2020). Effect of multiple hole distribution and shape based on particle flow on rocklike failure characteristics and mechanical behavior. *Advances in Civil Engineering, (6)*, 1–13.

[33]. AE, D., Gokay, M. (2016). Cuttability assessment of selected rocks through different brittleness values. *Rock Mechanics and Rock Engineering, 49*,1173–1190.

[34]. Liu, Q., Liu, J., Shi, K., Pan, Y., Huang, X., Liu, X., & Wei, L. (2016). Evaluation of rock brittleness indexes on rock fragmentation efficiency by disc cutter. *Chinese Journal of Rock Mechanics and Engineering, 35(3)*:498-510 (in Chinese).

[35]. Haeri, H., Shahriar, K., Fatehi Marji, M., & Moarefvand, P. (2014). On the Strength and Crack Propagation Process of the Pre-Cracked Rock-Like Specimens Under Uniaxial Compression. *Strength of Materials,46(1)*.

[36]. Haeri, H., (2015). Simulating the Crack Propagation Mechanism of Pre-Cracked Concrete Specimens Under Shear Loading Conditions. *Strength of Materials 47*, 618–632.

[37]. Haeri, H., (2015). Propagation mechanism of neighboring cracks in rock-like cylindrical specimens under uniaxial compression. *Geomechanics. Volume 51*.

[38]. Haeri, H., Sarfarazi, V. (2016). The deformable multilaminate for predicting the Elasto-Plastic behavior of rocks. *Computers and Concrete, 18(2)*, 201-214

[39]. Tian, Z., Tang, C., Yu, C., Liu, Y., Chen, S., & Jin, Y. (2022). Numerical Simulation Analysis of Mechanical Properties on Rock Brittle–Ductility Transformation Under Different Loading Rates. *Frontiers in Earth Science,* 10:825229.

[40]. Liang, Z., Song, W. (2021). Theoretical and Numerical Investigations of the Failure Characteristics of a Faulted Coal Mine Floor above a Confined Aquifer. *International Journal of Mine Water, 40 (2)*, 456–465.

[41]. Tang, S., Wang, J., & Tang, C. (2020). Identification of Microseismic Events in Rock Engineering by a Convolutional Neural Network Combined with an Attention Mechanism. *Rock Mechanics and Rock Engineering, 54(1)*, 47–69.

[42]. Tian, Z., Tang, C., Liu, Y., & Tang, Y. (2020). Zonal Disintegration Test of Deep Tunnel under Plane Strain Conditions. *International Journal of Coal Science & Technology, 7(2)*, 337–349.

[43]. Jiang, X., Ma, T., Okubo, S., Peng, S., Tang, Y., Chen, C., Wang, Z. (2017). Experimental Study of Generalized Stress Relaxation Characteristics of Rock under Different Confining Pressures. *Yantu Lixue/Rock and Soil Mechanics, 38*, 57–66.

[44]. Kang, Y., Jia, Y., Luo, Y., & Chen, J. (2017). Research on the Theoretical and Experimental Value of Azimuth Angle of the Fracture Surface for the Rock Subjected to Triaxial Compression. Sec. *Solid Earth Geophysics, 49(05)*, 665–670.

[45]. Wang, S., Xu, W., Wang, W., Wang, R., & Xiang, Z. (2017). The Statistical Damage Constitutive Model of Rocks and its Experiment. *Journal of Hohai University, 45(05)*, 464–470.

[46]. Zheng, Z., Zheng, H., Zhao, J., Liu, Z., Feng, G., & Qiu, Sh. (2023). Ductile–brittle quantitative evaluation of rock based on post-peak properties under true triaxial stress Geomech. *Geomechanics and Geophysics for Geo-Energy and Geo-Resources, 9(1)*.

[47]. Wong, T., Baud, P. (2012). The brittle-ductile transition in porous rock: A review. *Journal of Structural Geology, 44(52)*, 25–53.

[48]. Schopfer, M., Childs, C., & Manzocchi, T. (2013) Three-dimensional failure envelopes and the brittle-ductile transition. *Journal of Geophysical Research: Solid Earth, 118(4)*, 1378–1392.

[49]. Lyakhovsky, V., Zhu, W., & Shalev, E. (2015). Visco-poroelastic damage model for brittle-ductile failure of porous rocks. *Journal of Geophysical Research: Solid Earth, 120(4)*, 2179–2199.

[50]. Liu, W., Zhu, X., & Jing, J. (2018). The analysis of ductile-brittle failure mode transition in rock cutting. *Journal of Petroleum Science and Engineering, 163*, 311–319.

[51]. Aharonov, E., Scholz, C. (2019). The brittle-ductile transition predicted by a physics-based friction law. *Journal of Geophysical Research: Solid Earth, 124(3)*, 2721–2737.

[52]. Zhao, J., Feng, X., Zhang, X., & Yang, C. (2019). Brittle and ductile creep behavior of Jinping marble under true triaxial stress. *Engineering Geology, 258*, 105157.

[53]. Liu, S., Chen, H., Yuan, S., & Zhu, Q. (2020). Experimental investigation and micromechanical modeling of the brittle-ductile transition behaviors in low-porosity. *International Journal of Mechanical Sciences, 179*, 105654.

[54]. Davarpanah, M., Somodi, G., & Vásárhelyi, B. (2020). Experimental determination of the mechanical properties and deformation constants of Mórágy granitic rock formation (Hungary). *Geotechnical and Geological Engineering, 38(3)*, 3215–3229.

[55]. You, T., Waisman, H., & Zhu, Q. (2021). Brittle-ductile failure transition in geomaterials modeled by a modified phase-field method with a varying damage-driving energy coefficient. *International Journal of Plasticity, 136*, 102836.

[56]. Jacquey, A., Cacace, M. (2020). Multiphysics modeling of a brittle-ductile lithosphere: 2. Semi-brittle, semi-ductile deformation and damage rheology. *Journal of Geophysical Research: Solid Earth,125(1)*.

[57]. Su, C., Qiu, J., Wu, Q., & Weng, L. (2020). Effects of high temperature on the microstructure and mechanical behavior of hard coal. *International Journal of Mining Science and Technology, 30(5)*, 643–650.

[58]. Kim, B., Larson, M. (2021). Laboratory investigation of the anisotropic confinement-dependent brittle-ductile transition of a Utah coal. *International Journal of Mining Science and Technology, 31(1)*, 51–57.

[59]. Yaylacı, M., Abanoz, M., Yaylacı, E., Ölmez, H., Sekban, D., Birinci, A. (2022) Evaluation of the contact problem of functionally graded layer resting on rigid foundation pressed via rigid punch by analytical and numerical (FEM and MLP) methods. *Archive of Applied Mechanics, 92*, 1953–1971.

[60]. Yaylaci, M., Yaylacı, E., Özdemir, M., & Ay, S. (2022) Implementation of finite element and artificial neural network methods to analyze the contact problem of a functionally graded layer containing crack. *Steel and Composite Structures, 45(4*), 501-511.

[61]. Yaylaci, M., Yaylacı, E., Özdemir, M., Özturk, S., & Sesli, H. (2023) Vibration and buckling analyses of FGM beam with edge crack: Finite element and multilayer perceptron methods. *Steel and Composite Structures, 46(4)*, 565-575.

[62]. Stöcklin, J. (1968). Structural history and tectonics of Iran: a review. *Am Assoc Pet Geol Bull 52*:1229–1258.

[63]. Shahbazi, H., Siebel, W., Pourmoafee, M., Ghorban,i M., Sepahi, A., Shang, CK., & Vousoughi

Abedini, M. (2010). Geochemistry and U–Pb zircon geochronology of the Alvand plutonic complex in Sanandaj–Sirjan Zone (Iran): new evidence for Jurassic magmatism. *Journal of Asian Earth Sciences,39*, 668–683.

[64]. Valizadeh, M., Cantagrel, J. (1975). Premières données radiométriques (K–Ar et Rb–Sr) sur les micas du complexes magmatique du Mont Alvand, Pres Hamadan (Iran occidental). *Comptes Rendus de l'Academie des Sciences, Paris 281*, 1083–6.

[65]. Eshraghi, S., Mohammadi Gharai, M. (2003). Geological Map of Tuyserkan 1/100000, *Geological Survey and Mineral exploration of Iran*, Tehran.

[66]. Baharifar, A., Moinevaziri, H., Bellon, H., & Piqué, A. (2004). The crystal-line complexes of Hamadan (Sanandaj–Sirjan zone, western Iran): metasedimentary Mesozoic sequences affected by Late Cretaceous tectono-metamorphic and plutonic events. *Comptes Rendus Geoscience, 336*,1443–1452.

[67]. Sepahi, A., Whitney, D., & Baharifar, A. (2004). Petrogenesis of anda-lusite–kyanite–sillimanite veins and host rocks, Sanandaj–Sirjan metamorphic belt, Hamadan. *Journal of Metamorphic Geology, 22*,119–134.

[68]. Stocklin, J., Setudenia, A. (1972). Lexique stratigraphique international, vol.III. Paris*: Centre National de la Recherche Scientifique*, 75 pp.

[69]. Sepahi, A., Salami, S., Lentz, D., McFarlane, C., Maanijou, M. (2018). Petrography, geochemistry, and U–Pb geochronology of pegmatites and aplites associated with the Alvand intrusive complex in the Hamedan region, Sanandaj–Sirjan zone, Zagros orogen (Iran). *International Journal of Earth Sciences, 107*, 1059–1096.

[70]. Undul, O. (2016). Assessment of mineralogical and petrographic factors affecting petro-physical properties, strength and cracking processes of volcanic rocks. *Engineering Geology, 210(2)*.

[71]. Ozturk, C., Nasuf, E. (2013). Strength classification of rock material based on textural properties. *Tunnelling and Underground Space Technology, 37*,45–54.

[72]. Tandon, R., Gupta, V. (2013). The control of mineral constituents and textural characteristics on the petrophysical & mechanical (PM) properties of different rocks of the Himalaya. *Engineering Geology,153*, 125–143.

[73]. Ündül, O. (2016). Assessment of mineralogical and petrographic factors affecting petrophysical properties, strength and cracking processes of volcanic rocks. *Engineering Geology, 210*,10–22.

[74]. Howarth, D., Rowlands, J. (1987). Quantitative assessment of rock texture and correlation with drillability and strength properties. *Rock Mechanics and Rock Engineering, 20*, 57–85.

[75]. Ozturk, C. (2004) The assessment of rock cutability, and physical and mechanical rock properties from a texture coefficient. *Journal of the Southern African Institute of Mining and Metallurgy, 104(7)*, 397–403.

[76]. Alber, M., Kahraman, S. (2009). Predicting the uniaxial compressive strength and elastic modulus of a fault breccia from texture coefficient. *Rock Mechanics and Rock Engineering, 42*,117–127.

[77]. Singh, T., Verma, A. (2012). Comparative analysis of intelligent algorithms to correlate strength and petrographic properties of some schistose rocks. *Engineering with Computers, 28*,1–12.

[78]. Ozturk, C., Nasuf, E., & Kahraman, S. (2014). Estimation of rock strength from quantitative assessment of rock texture. *Journal of the Southern African Institute of Mining and Metallurgy, 114(6)*, 471-480.

[79]. Roduit, N. (2009). JMicroVision: image analysis toolbox for measuring and quantifying components of high-definition images. Version 1.2.7. Software available for free download at http:// www.jmicrovision.com.

[80]. Dreyer, W. (1973) The Science of Rock Mechanics. Part I. The Strength Properties of Rocks. Series on Rock and Soil Mechanics, *Trans Tech Publications*, Clausthal.

[81]. Aligholi, S. Lashkaripour, G., & Ghafoori, M. (2018). Estimating engineering properties of igneous rocks using semi-automatic petrographic analysis. *Bulletin of Engineering Geology and the Environment, 78*. 2299-2314.

[82]. Peng, J. Wong, N., & Teh, C. (2017). Influence of grain size heterogeneity on strength and micro-cracking behavior of crystalline rocks. *Journal of Geophysical Research: Solid Earth, 122*, 1054-1073.

[83]. Mogi, K. (1966). Pressure dependence of rock strength and transition from brittle fracture to ductile flow. *Bulletin of the Earthquake Research Institute, 44*, 215-232.

[84]. Hucka, V., Das, B. (1974). Brittleness determination of rocks by different methods. *International Journal of Rock Mechanics and Mining Sciences & Geomechanics Abstracts, 11*, 389–392.

[85]. Singh, S. (1985). Brittleness and the mechanical winning of coal. *Mining Science and Technology, 3*, 173–180.

[86]. Heidari, M., Khanlari, G., Torabi Kaveh, M., Kargarian, S., & Saneie, S. (2014). Effect of porosity on rock brittleness. *Rock Mechanics and Rock Engineering, 47*, 785–790.

[87]. Mohammadi, S., Torabi Kaveh, M., & Bayati, M. (2015). Prediction of TBM penetration rate using intact and mass rock properties (case study, Zagros long tunnel, Iran*). Arabian Journal of Geosciences, 8(6)*, 3893-3904.

انجمن مهندسی معدن ایران
نشریه مهندسی معدن و محیط زیست
نشانی نشریه: www.jme.shahroodut.ac.ir
دانشگاه صنعتی شاهرود

تأثیر اندازه کانی، ضریب بافت، شکل‌پذیری و شکنندگی در ایجاد حفره در نمونه سنگهای گرانیتی

آرام اردلان زاده[۱]، سید داود محمدی[۱*]، وهاب سرفرازی[۲] و حسین شهبازی[۱]

۱. گروه زمین شناسی، دانشگاه بوعلی سینا، همدان، ایران
۲. دانشکده مهندسی معدن، دانشگاه صنعتی، همدان، ایران

اطلاعات مقاله

تاریخ ارسال: ۲۰۲۴/۱۰/۱۹
تاریخ داوری: ۲۰۲۴/۱۲/۰۸
تاریخ پذیرش: ۲۰۲۴/۱۲/۰۸

DOI: 10.22044/jme.2024.15230.2913

کلمات کلیدی

گرانیت
بافت سنگ
حفره سنگ
ضریب بافتی
شاخص شکنندگی

چکیده

ایجاد حفره در سنگ ها با استفاده از روش های مختلف چالش های مختلفی را به همراه دارد. در این تحقیق سعی شد تا این ویژگی ها و مشکلات موجود در ایجاد حفره بر اساس بافت و شکنندگی سنگ مورد بررسی قرار گیرد. برای این منظور، از باتولیت گرانیتی الوند همدان، چندین نمونه مغزه گرفته شد و شاخص‌های سنگ‌شناسی و بافتی سنگ‌ها تعیین شد. نمونه ها شامل چهار نوع بافت بوده که از دانه درشت تا ریزدانه متغیر است. ضرایب بافت (TC) برای چهار نوع سنگ (G1 تا G4) به ترتیب ۱.۷۰۹، ۱.۷۳۰، ۱/۷۷۴ و ۱/۶۹۷ بوده است. شاخص شکنندگی‌نیز (B1) برای چهار نوع سنگ (G1 تا G4) به ترتیب ۹/۱۳، ۱۱/۰۱، ۱۲/۰۷و ۱۰/۶۵ به دست آمده است. پس از آن با استفاده از مته الماسه در هر نمونه مغزه سنگی یک حفره ایجاد گردید و در پایان حفاری از پشت هر حفره نمونه، یک گودال شکستگی جدا شد. نتایج نشان می دهد که با کاهش اندازه کانی، عمق گودال شکستگی نیز کاهش می یابد و در بافت پورفیری، عمق گودال شکستگی بین مقدار عمق گودال شکستگی سنگ های درشت دانه و دانه متوسط قرار می گیرد. با افزایش ضریب بافت (TC) و شکنندگی نمونه های سنگ، عمق گودال شکستگی کاهش می یابد و در بافت پورفیری، عمق گودال شکستگی بین اعماق گودال شکستگی سنگ های درشت دانه و دانه متوسط باقی می ماند. در نهایت، نتایج آزمایش‌های آزمایشگاهی نشان می‌دهد که ایجاد حفره ها توسط مته الماسه، به منظور مطالعه تأثیر حفره ها بر رفتار سنگ ها، می‌تواند باعث آسیب به سنگ‌ها گردد.

نویسنده مسئول مکاتبات: d.mohammadi@basu.ac.ir (س.د. محمدی)